The Relationship between Energy Additivity and the Equivalent Group

Joseph R. Murdoch* and Douglas E. Magnoli

Contribution from the Department of Chemistry, University of California, Los Angeles, California 90024. *Received April 10, 1980*

Abstract: The idea of the equivalent group which can be transferred from molecule to molecule as an intact unit has played a key role in understanding molecular structure and reactivity. In the present paper it is shown that introducing a substituent into a molecule can produce substantial shifts in electron density, both in the substituent and in the rest of the molecule. Based on current concepts, one would not expect to find a high degree of energy additivity in such a situation. However, these changes in electron density can be mutually compensating, so that energy and bond length additivity are observed anyway. A surprising new result is that energy additivity does *not* require equivalent, transferable groups which maintain constant electronic structure in different molecules. This finding has important implications for any theory attempting to describe multiple substituent effects since it may be necessary to explicitly recognize interactions between groups and changes in electronic structure even when energy additivity is observed. These phenomena are examined from the viewpoint of a theory of nuclear substitution, which has been presented previously. The spatial distributions of electron density, orbital energy, and kinetic energy are used to probe the relationship between group transferability and energy additivity.

Introduction. The Equivalent Group: A Ubiquitous Concept

Ever since Dalton[1] proposed that molecules are composed of atoms combined in definite proportions, the concept of the equivalent group has provided a focal point in rationalizing multiple substituent effects on molecular structure and reactivity. The structure of the equivalent group is thought to be an intrinsic property of the group and independent of the other structural units in the molecule. Consequently, the heat of formation of a molecule composed of equivalent groups can be expressed in terms of additive contributions of each group. This approach has been surprisingly successful for a wide variety of compounds[2] and has even been applied to bicyclic materials containing strained rings.[3] It has also been recognized that interactions can occur between molecular components and that these interactions require additional contributions to the heat of formation. It is interesting that interactions between groups can frequently be treated as additive effects. For example, gauche interactions between alkyl groups are often additive in such a way that each gauche interaction contributes a fixed amount to the heat of formation.[4]

Molecular mechanics and force-field approaches[5] also preserve the basic idea of the equivalent group. Nonbonded interactions between two atoms may be described in terms of potential functions[5] so that the internuclear distance and type of atoms are the only variables affecting the interaction. Nonbonded interactions may result in deviations from standard bond lengths and bond angles, and this effect also requires additional increments to the heat of formation. Again, these contributions depend only on the distortion of a specific bond length or bond angle and are independent of other interactions or geometric changes in the molecule. The high degree of success[5] at predicting heats of formation has resulted in a general acceptance of the idea that fragments can maintain constant electronic and geometric structure in different molecules. The equivalent group has gained further support from theoretical treatments which reproduce ab initio energies and properties of large molecules by transferring matrix elements or localized orbitals from simpler structures.[6]

The equivalent group concept is also fundamental to the Hammett equation[7] and other forms of linear free-energy relationships.[8] Hammett suggested that the effect of replacing a substituent on the pK_a of benzoic acids could be described in terms of a "substituent" parameter (σ) and a "reaction" parameter, ρ. According to Hammett,[7] the acid dissociation constant of a substituted benzoic acid is given by

$$\log (K_a/K_0) = \sigma\rho \qquad (1)$$

where K_0 is the acid dissociation constant of benzoic acid. σ is regarded as an intrinsic property of the substituent and independent of the structure of the rest of the molecule. Likewise, ρ is looked upon as an intrinsic property of the group undergoing reaction (e.g., $-CO_2H \rightarrow -CO_2^-$) and is independent of substituent.

Numerous refinements[8a-e] of the Hammett equation have appeared since Hammett's original proposal. Forsyth[8f] has presented a simple extension which provides a rather remarkable correlation of rates for aromatic substitution and side-chain solvolysis reactions of benzene, naphthalene, furan, thiophene, and other aromatic derivatives.

Forsyth treats field and resonance interactions of the substituents in terms of two parameters (D and E^+). The D and E^+ parameters are regarded as intrinsic properties of the substituent and are assumed to be independent of both the specific aromatic ring to which the substituents are attached and the relative importance of the field and resonance effects. It is hard to avoid questioning these assumptions, but one is faced with the fact that Forsyth's model provides an impressive correlation of solvolytic and electrophilic substitution reactions in a wide variety of aromatic systems.

The equivalent group models all have one common element: characteristic parameters are assigned to certain structural units within the molecule, and these parameters remain unchanged even when interactions occur between the structural units. The

(1) J. R. Partington, "A Short History of Chemistry," 3rd ed., Harper and Brothers, New York, 1960, p 173.

(2) (a) S. W. Benson, "The Foundations of Chemical Kinetics", McGraw-Hill, New York, 1960, p 670. (b) D. R. Stull, E. F. Westrum, Jr., and G. C. Sinke, "The Chemical Thermodyanmics of Organic Compounds", Wiley, New York, 1969.

(3) (a) J. Gasteiger and O. Dammer, *Tetrahedron*, **34**, 2939 (1978). (b) D. Van Vechten and J. F. Liebman, *Isr. J. Chem.* **21**, 105 (1981).

(4) A. J. Kalb, A. L. H. Chung, and T. L. Allen, *J. Am. Chem. Soc.*, **88**, 1938 (1966).

(5) N. L. Allinger, *Adv. Phys. Org. Chem.*, **13**, 1 (1976).

(6) B. O'Leary, B. J. Duke, and J. E. Eilers, *Adv. Quantum Chem.* **9**, 1 (1975).

(7) L. P. Hammett, "Physical Organic Chemistry", McGraw-Hill, New York, 1940.

(8) (a) J. E. Leffler and E. Grunwald, "Rates and Equilibria of Organic Reactions", Wiley, New York, 1963. (b) S. Ehrenson, *Prog. Phys. Org. Chem.*, 195 (1965). (c) C. D. Ritchie and W. F. Sager, *ibid.*, 323 (1965). (d) C. D. Johnson, *Chem. Rev.*, **75**, 755 (1975). (e) B. Giese, *Angew. Chem., Int. Ed. Engl.*, **16**, 125 (1977). (f) D. A. Forsyth, *J. Am. Chem. Soc.*, **95**, 3594 (1973).

(9) One approach to this problem is to apply equivalent group assumptions to the *derivative* of the energy change and to obtain, after integration, a nonlinear relationship between two free energy quantities. This leads to a simple model for a rate–equilibrium relationship which quantitatively accounts for many features of proton transfer and other reactions. However, such a semiempirical solution is not as convincing as one derived from a rigorous ab initio foundation. J. R. Murdoch, *J. Am. Chem. Soc.*, **94**, 4410 (1972).

0002-7863/82/1504-2782$01.25/0

equivalent group approach can account for additivity and even some degree of nonadditivity. However, the range of nonadditivity is necessarily limited due to the lack of a mechanism for introducing systematic changes in the substituent parameters as interactions become progressively larger.[9]

Theoretical treatment of nonlinear substituent effects will require understanding of how interactions between structural units in a molecule alter the properties of the equivalent group and limit the degree of transferability. The solution to this problem has assumed a significance that extends well beyond a simple refinement of the equivalent group approximation. In recent years, there have been an increasing number of curved rate–equilibrium relationships for a wide variety of reactions, including proton transfer.[10] The curvature is an example of a nonlinear substituent effect and of a breakdown in the equivalent group concept. Through various semiempirical relationships, such as Marcus' equation,[9,11] it is possible to relate this curvature[10] to various factors contributing to the overall observed barrier for the reaction. These factors include bond making and bond breaking, diffusion, solvent reorganization, orientation, and molecular distortions. One implication of these results[10] is that making and breaking chemical bonds is often *less* important than these other factors as a contributor to the overall barrier. If valid, this result is of great significance for many aspects of mechanistic chemistry and holds important implications for the problem of designing catalysts for accelerating solution phase reactions. A catalyst which works by altering the way bonds are formed and broken involves fundamentally different principles than a catalyst which compensates for reorganization of solvent, orientation, or conformational changes. Unfortunately, no direct experimental evidence is available for assessing the relative importance of bond formation and other factors to the overall barrier, and so present conclusions[10] must remain as tantalizing deductions derived from a theory[9,11] based on assumptions of questionable applicability.

The motivation for examining nonlinear substituent effects is not to simply reduce the scatter in force-field calculations and in Hammett-type relationships, but to provide a reasonable theoretical framework for evaluating the present conclusions regarding the relatively minor importance of bond formation to reaction barriers for certain classes of reactions. The first step in the development of a theory of nuclear substitution is presented in the previous paper,[12] and the results have been used[13] to evaluate the importance of various contributions to reaction barriers. Initially it was thought that nonlinear substituent effects could be treated by extending equations based on additivity and the equivalent group formalism. However, it became apparent that the equivalent group approximation breaks down *before* energy additivity, so that energy additivity persists even *after* the electronic structure of the various molecular units has been altered by mutual interactions. Such behavior is totally unexpected on the basis of previous models of substituent effects. This phenomenon is apparently general, and in the present paper, the fundamental principles behind this unusual behavior are examined through the hemistructural relationship.

The Hemistructural Relationship

In the previous paper,[12] the effect of a relatively simple geometry constraint on the molecular wave function and energy was explored. This geometry constraint relates a "hybrid" structure, A–B–C, to two "parent" structures, A–B–A and C–B–C. A coordinate system is chosen so that the nuclear coordinates of the "A" fragment are the same in A–B–C and A–B–A. A similar constraint operates on the "B" and "C" fragments. This type of geometric arrangement was termed[12] the hemistructural relationship and can be regarded as a form of geometry additivity. An important consequence of the hemistructural relationship is the *exact* transferability of all integrals necessary for defining the Hartree–Fock wave function.[12,14]

Integral transferability leads to the useful result that the nuclear-electron attraction matrix elements for C–B–C, $(V_{ne}^{ij})_{CBC}$, can be expressed[12] as an additive sum of three contributions:

$$(V_{ne}^{ij})_{CBC} = (V_{ne}^{ij})_{ABA} + (\delta V_{ne}^{ij})_{CBA} + (\delta V_{ne}^{ij})_{ABC} \quad (2)$$

where

$$(\delta V_{ne}^{ij})_{CBA} = (V_{ne}^{ij})_{CBA} - (V_{ne}^{ij})_{ABA} \quad (3)$$

$$(\delta V_{ne}^{ij})_{ABC} = (V_{ne}^{ij})_{ABC} - (V_{ne}^{ij})_{ABA} \quad (4)$$

It has also shown that these additive changes in V_{ne}^{ij} could[12] lead to a similar additivity in the MO coefficients for C–B–C (ψ_ν)

$$\psi_\nu = \sum_m (a^0{}_{\nu m} + a'_{\nu m})\phi_m \quad (5)$$

where the corresponding unperturbed MO for A–B–A is given by

$$\psi_\nu{}^0 = \sum_m a^0{}_{\nu m}\phi_m \quad (6)$$

and ϕ_m represents a complete set of nuclear-*independent* basis functions.[14] The coefficient additivity allows $a'_{\nu m}$ to be expressed as

$$a'_{\nu m} = a^r{}_{\nu m} + a^l{}_{\nu m} \quad (7)$$

where $a^r{}_{\nu m}$ is the change in coefficients for the perturbation A–B–A → A–B–C, while $a^l{}_{\nu m}$ is the change in coefficients for A–B–A → C–B–A.

When $a'_{\nu m}$ (eq 7) is substituted into the expression for the kinetic energy[12]

$$T = 2\sum_\gamma^{occ}\sum_i\sum_j (a^0{}_{\nu j} + a'_{\nu j})T_{ij}(a^0{}_{\nu i} + a'_{\nu i}) \quad (8)$$

it is seen that the linear terms contributing to T (i.e., $a'_{\nu j}T_{ij}a^0{}_{\nu i}$) are a function only of $a'_{\nu j}$ and respond independently to separate changes in nuclear charge and position. Consequently, the linear contribution to T is additive.

The behavior of the kinetic energy is important since the virial theorem requires that the total energy and the kinetic energy respond in equal but opposite fashion to substituent changes.[12] While the virial theorem requires that the total potential energy ($V = V_{ne} + V_{ee} + V_{nn}$) show the same degree of additivity as T and E, this does not apply to the individual terms V_{ne}, V_{ee}, and V_{nn}.[12] Consequently, it is possible to observe a high degree of additivity in E, T, and V, even though V_{ne}, V_{ee}, and V_{nn} are essentially nonadditive. One consequence of these relationships is that the total energy ($E = T + V_{ne} + V_{ee} + V_{nn}$) will always be more additive than the orbital energy ($E_0 = T + V_{ne} + 2V_{ee}$).[12]

According to standard forms of perturbation theory,[15] energy additivity is associated with first-order energy differences and no change in MO coefficients. Changes in MO coefficients produce second-order changes in energy which are nonadditive.[12] Consequently, the degree of energy additivity has been thought to depend on the degree to which changes in MO coefficients and second-order energy corrections are negligible. Group transferability has generally been regarded as a necessary prerequisite

(10) For leading references, see: J. R. Murdoch, *J. Am. Chem. Soc.*, **102**, 71 (1980).

(11) (a) R. A. Marcus, *J. Phys. Chem.*, **72**, 891 (1968). (b) A. O. Cohen and R. A. Marcus, *ibid.*, **72**, 4249 (1968).

(12) J. R. Murdoch, *J. Am. Chem. Soc.*, **104**, 588 (1982).

(13) (a) D. E. Magnoli and J. R. Murdoch, *J. Am. Chem. Soc.* **103**, 7465 (1981). (b) J. R. Murdoch and D. E. Magnoli, *J. Am. Chem. Soc.*, in press.

(14) The integral transferability leads to a simplified behavior of the Hartree–Fock wave function and energy. The transferability was demonstrated using a complete basis set where the basis functions are independent of nuclear charge and position. The transferability is basis set dependent, but the resulting behavior of the Hartree–Fock wave function holds for *all* complete basis sets regardless of integral transferability. The immediate value of integral transferability is not as a computational advantage, but as a means of exposing the relationship between the wave functions and energy of ABA, ABC, and CBC. Integral transferability is obviously an appealing idea for executing actual calculations, but it involves a number of tradeoffs which are presently undergoing careful consideration.

(15) (a) F. L. Pilar, "Elementary Quantum Chemistry", McGraw-Hill, New York, 1968. (b) M. J. S. Dewar, "The Molecular Orbital Theory of Organic Chemistry", McGraw-Hill, New York, 1969.

Table I. Calculated[a] Energy Components for Proton-Bound Rare Gas Dimers

	NeHNe$^+$	NeHAr$^+$	ArHAr$^+$
E_0, au	−153.467 620	−402.282 828	−651.101 725
T	253.510 356	648.128 243	1042.746 459
V_{ne}	−675.555 372	−1638.342 345	−2616.749 610
V_{ex}	−24.675 115	−42.753 512	−60.850 379
V_{co}	158.963 814	336.719 148	522.301 092
V_{nn}	34.245 961	48.119 952	69.805 928
E	−253.510 357	−648.128 513	−1042.746 510
η	1.010 393 87	1.000 016 998[b]	1.009 675 95
r_{NeH}, bohr	2.044 036 66	2.044 036 66	
r_{HAr}, bohr		2.836 435 33	2.836 435 33

[a] Standard 3G exponents are scaled by η^2. Gaussian lobe functions replace Cartesian p Gaussians (J. L. Whitten, *J. Chem. Phys.*, 44, 359 (1966)). [b] The orbital exponents for NeHAr$^+$ were taken from the corresponding scaled values for NeHNe$^+$ and ArHAr$^+$ (except for the proton whose exponents are the average of those for the proton in the two symmetrical structures) and then scaled by $(1.000\ 016\ 998)^2$.

for energy additivity.[16] The problem with basing a theory of nuclear substitution on this foundation is that there are many examples of additivity to within a few tenths of a kilocalorie, even though it is apparent from other properties that substantial changes in MO coefficients have taken place. This prompted a new theoretical treatment[12] which shows that while energy additivity can be associated with coefficient additivity (eq 7), there is no absolute requirement that constant electron density be maintained in a particular region of space or over a specific molecular orbital. This carries the important implication that energy additivity is *not* linked to the degree of structural transferability. This result is unprecedented and in the following sections, the relationship between additivity and transferability is examined by analyzing the behavior of the various energy components (T, V_{ne}, V_{ee}, V_{nn}) and by comparing the spatial distribution of electron density, orbital energy, and kinetic energy.

Energy Additivity and Transferability. Proton-Bound Rare Gas Atoms

Initially, it was desirable to examine a simple system where transferability might have a good chance of adequately describing energy additivity. Consequently, proton-bound rare gas dimers were the first molecules to be studied, since a minimum of electronic and geometric reorganization is expected[17] in the series XHX$^+$, XHY$^+$, and YHY$^+$ (X and Y are rare gas atoms).

Calculations were carried out with GAUSSIAN 70[18] and PROMETHEUS X,[19] using Pople's standard 3G basis set as well as a rescaled version which is described in Table I. The energies and optimized geometries (3G basis) of X, H–X$^+$, and XHY$^+$ (X, Y = He, Ne, Ar) are reported in the following paper.[13b] Since the calculated energy of NeHAr$^+$ was found to be within 0.1 kcal of the mean energy of NeHNe$^+$ and ArHAr$^+$, this system was examined further. It is interesting to note that the optimized geometry of NeHAr$^+$ is close to the hemistructural geometry: the H–Ne distance is shorter by 0.004 Å and the H–Ar distance is longer by 0.011 Å relative to the hemi-structural geometry.

In general, the virial theorem will not be satisfied for calculations employing a minimal basis set such as 3G, unless the exponents and bond distances are rescaled. Procedures for scaling approximate Hartree–Fock wave functions have been reported,[20] but it was found that the scaled wave function and the wave function obtained from another calculation with the new scaling factors were invariably in poor agreement.

The calculations presented in Table I use a new scaling procedure which will be described elsewhere. For Pople's standard 3G basis set, the scaling factors and bond distances reported in Table I yield wave functions satisfying the virial theorem ($E/T + 1 = 0$) to better than 10^{-6}.

The scaled energies show a high degree of additivity: the energy of NeHAr$^+$ is 0.05 kcal lower than the mean energy of NeHNe$^+$ and ArHAr$^+$. In striking contrast, V_{ne} for NeHAr$^+$ deviates from the mean by +4900.87 kcal, while ($V_{ee} + V_{nn}$) diverges in the opposite direction by −4900.81 kcal. The near cancelation of repulsive and attractive terms is required by the virial theorem[12] since the total potential energy and total energy are related as $E = V/2$.

A. Energy Additivity. A Classical Electrostatic Viewpoint. The high degree of additivity for E, T, and V (Table II) suggests that we examine several simple models for rationalizing additivity. One approach is to test the possibility that Ar and Ne in the three structures are behaving as essentially neutral, unpolarized atoms (or high-order multipoles), so that Ar/Ne, Ar/Ar, and Ne/Ne interactions are negligible. If this were the case, the classical electrostatic energy, representing the total attractions and repulsions of the nuclei and the quantum mechanical electron distribution, should show a degree of additivity comparable to the quantum mechanical total energy. The classical electrostatic energy can be obtained from E by subtracting the exchange contribution (V_{ex}) from V_{ee}.[21] V_{ex} for NeHAr$^+$ deviates from the mean V_{ex} for NeHNe$^+$ and ArHAr$^+$ by +5.8 kcal, so that the classical electrostatic energy is nonadditive by −5.85 kcal. Considering that the total range of energy covered by these structures is over 490 000 kcal, this degree of additivity is quite impressive,

Table II. Additivity of Energy Components. Mean Deviations[a] for Proton-Bound Rare Gas Dimers (ArHNe$^+$)

	mean deviation, kcal		mean deviation, kcal
ΔE_0	+1.157	ΔV_{co}[b]	−2455.598
ΔT	−0.103	ΔV_{nn}	−2451.010
ΔV_{ne}	+4900.867	ΔE	−0.050
ΔV_{ex}[b]	+5.794		

[a] Mean deviation equals the quantity calculated for ArHNe$^+$ minus the corresponding average quantity for ArHAr$^+$ and NeHNe$^+$. [b] The total electron/electron repulsion (V_{ee}) is given by $V_{ee} = V_{ex} + V_{co}$, where V_{ex} is the exchange energy and V_{co} is the Coulomb energy.

Table III. Population Analysis[a] for NeHNe$^+$, NeHAr$^+$, and ArHAr$^+$

	NeHNe	NeHAr	ArHAr
1s	1.999 393 52	1.999 392 16	
2s	1.973 567 67	1.973 216 75	
$2p_x$	1.737 118 33	1.705 955 61	
$2p_y$	2.00	2.00	
$2p_z$	2.00	2.00	
1s		1.999 973 25	1.999 973 36
2s		1.999 139 88	1.999 143 82
$2p_x$		1.994 511 30	1.993 951 65
$2p_y$		2.00	2.00
$2p_z$		2.00	2.00
3s		1.986 947 36	1.986 137 19
$3p_x$		1.731 135 24	1.690 575 01
$3p_y$		2.00	2.00
$3p_z$		2.00	2.00
H 1s	0.579 840 96	0.609 718 49	0.660 437 93

[a] Scaling factors are the same as those from Table I. Scaling has a negligible effect on the population analysis.

(16) (a) T. L. Allen and H. Shull, *J. Chem. Phys.*, **35**, 1644 (1961). (b) M. Levy, W. J. Stevens, H. Shull, and S. Hagstrom, *ibid.*, **61**, 1844 (1974). (c) R. F. W. Bader and P. M. Beddall, *Chem. Phys. Lett.*, **8**, 29 (1971). (d) R. F. Bader and G. R. Runtz, *Mol. Phys.*, **30**, 117 (1975).

(17) (a) V. Bondybey, P. K. Pearson, and H. F. Schaefer III, *J. Chem. Phys.*, **57**, 1123 (1972). (b) P. S. Julienne, M. Krauss, and A. C. Wahl, *Chem. Phys. Lett.*, **11**, 16 (1971).

(18) W. J. Hehre, W. A. Lathan, R. Ditchfield, M. D. Newton, and J. A. Pople, *QCPE*, **11**, 236 (1973).

(19) PROMETHEUS X is an experimental SCF-MO program now under development at UCLA. It will be described in detail elsewhere.

(20) E. Scarzafava and L. C. Allen, *J. Am. Chem. Soc.*, **93**, 311 (1971).

(21) S. Wolfe and A. Rauk, *J. Chem. Soc. B*, 136 (1971).

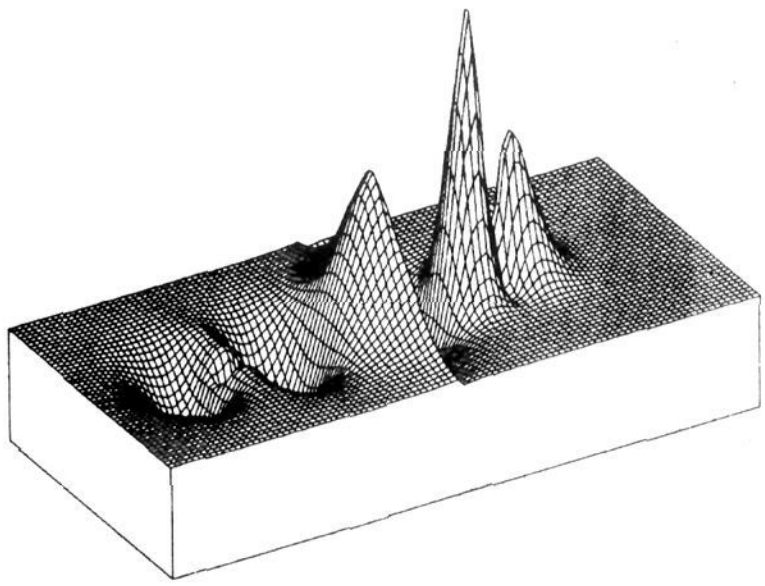

Figure 1. Projected electron density difference plot for $ArHNe^+$. The figure is constructed by separately placing $NeHNe^+$, $ArHNe^+$, and $ArHAr^+$ in the xy plane and integrating the electron density along the z axis from the surface of the plane to ∞. Each molecule is divided in half through the hydrogen and the difference between the electron density distribution of the Ar fragment in the parent and the Ar fragment in the hybrid is plotted in the left half of the grid. The corresponding differences for Ne appear in the right half of the grid. The maximum equals 0.00892 electron/bohr^2.

but it is also clear that near additivity of the classical electrostatic energy does not explain the even higher additivity observed for E, T, and V.[22]

B. Energy Additivity. The Orbital Energy. The orbital energy of $NeHAr^+$ is additive to within 1.16 kcal. The deviation is about 20 times the discrepancy observed for the total energy and is in qualitative agreement with previous expectations.[12] Additive total energies cannot be explained by invoking additive orbital energies.[12]

C. Energy Additivity and the Equivalent Group. Electron Density Distribution. It would also be interesting to examine the equivalent group model as a rationalization for additivity. In Table III, the Mulliken population analyses for $NeHNe^+$, $NeHAr^+$ and $ArHAr^+$ are listed. The major orbitals contributing to bonding are the Ne $2p_x$, Ar $3p_x$, and H 1s where the $\bar{x}$ direction lies along the internuclear axis. The Mulliken analysis shows a reduced population (by 0.031) for the Ne $2p_x$ orbital of $NeHAr^+$ relative to $NeHNe^+$, while the population for Ar $3p_x$ increases (by 0.041) on going to the hybrid structure. The H 1s population for $NeHAr^+$ (0.6097) is bracketed by the corresponding populations for $NeHNe^+$ (0.5798) and $ArHAr^+$ (0.6604). The overall pattern is not consistent with a constant wave function and transferable groups, but with small increases in density in one region and compensating decreases in another region.

This conclusion is reinforced by examining differences in the spatial distribution of electron density as seen in Figure 1. Figure 1 is constructed by placing each molecule in the xy plane and integrating the electron density along the z axis from the surface of the plane to ∞.[23] Each molecule is divided in half through the hydrogen and the difference between the electron density

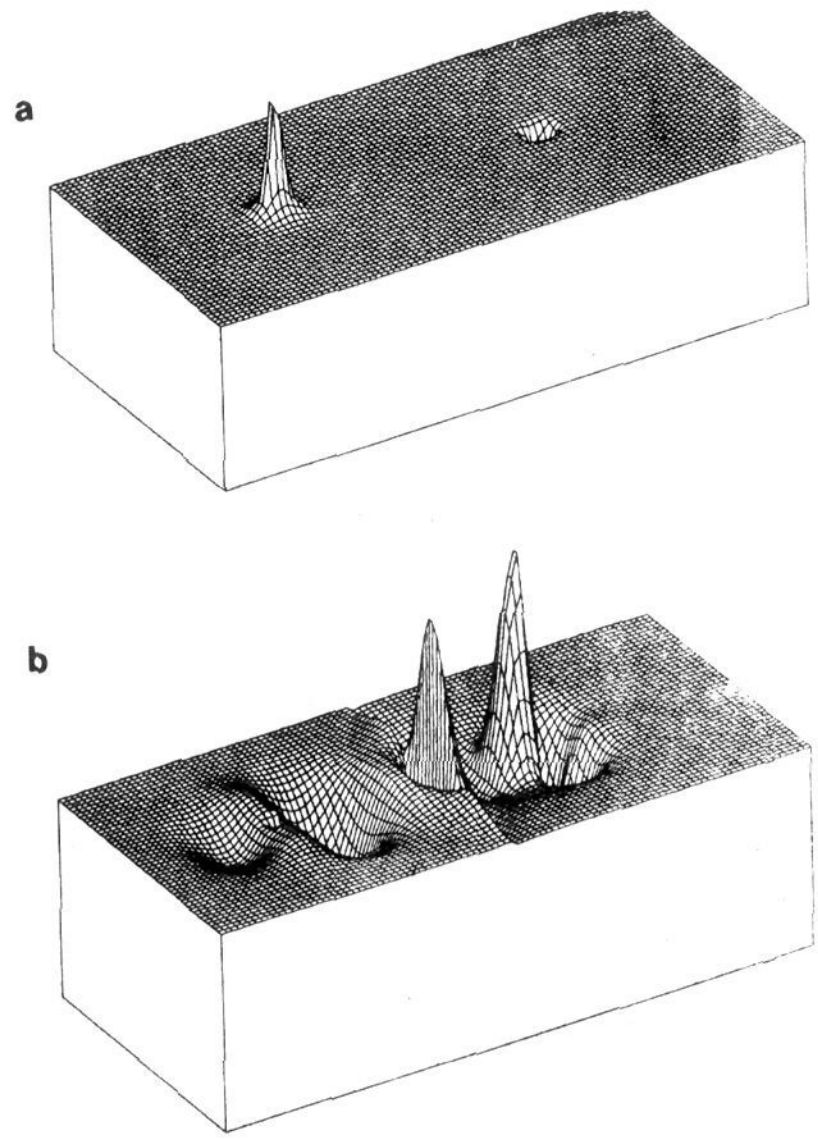

Figure 2. Projected orbital energy difference plot for $ArHNe^+$. The orbital energy is evaluated as a function of the spatial coordinates according to eq 10, and projected differences are plotted as in Figure 1. (a) Core orbitals, maximum equals 0.499 au/bohr^2. (b) Valence orbitals, maximum equals 0.00868 au/bohr^2. The integration mentioned in the text refers to the combined sum of core and valence orbitals.

distribution of the Ar fragment in the parent and the Ar fragment in the hybrid is plotted in the left half of the grid. The corresponding differences for Ne appear in the right half of the grid. The overall pattern is one of small but compensating changes in electron density in different spatial regions. For example, the dip in Figure 1 near the Ar region corresponds to about 0.04 e compared to 18 e assigned to this half of the grid for $ArHAr^+$. The pronounced rise near the Ar half of the proton corresponds to roughly 0.025 compared to 0.33 e assigned to the Ar half of the proton in $ArHAr^+$. These assignments have been based on the Mulliken analysis and not on partial integration over the surface of the grid. Nonetheless, they serve to emphasize that the overall changes in electron distribution are relatively small (0.2% to 8%) and that decreases in one region are offset by increases in another region.

D. Energy Additivity and the Equivalent Group. Spatial Distribution of Orbital Energy. The consequences of these compensating increases and decreases of electron density on energy additivity can be seen by plotting out differences in the spatial distribution of energy. The energy corresponding to the exact wave function is given by

$$E = \int \Psi H \Psi \, d\tau \tag{9}$$

The integrand, $\psi H \psi \, d\tau$, can be interpreted as the energy contribution from volume element $d\tau$ and can be assigned a spatial coordinate just as charge density can be assigned a spatial coordinate. If H is the Fock operator and ψ_i is one of the Fock eigenfunctions,

$$dE_i = \psi_i H \psi_i \, d\tau = \psi_i E_i \psi_i \, d\tau = (E_i)(\psi_i \psi_i \, d\tau) \tag{10}$$

Equation 10 gives us the interesting result that the orbital energy contribution from volume element $d\tau$ is equal to the fraction of electron density in the volume element times the orbital energy

(22) The classical electrostatic energy was also calculated in a self-consistent fashion by allowing the iterative Hartree–Fock procedure to continue without the contribution of the exchange integrals. This method converged for the systems examined here and invariably resulted in a higher degree of nonadditivity. The iterative calculations were performed with the standard 3G basis and are not scaled. The total energy (quantum mechanical) of $NeHAr^+$ deviates by only 0.1 kcal from the mean, while the classical energy for the quantum mechanical charge distribution deviates by −6.0 kcal from the mean. These results are comparable to those obtained with the scaled basis set. The "self-consistent" classical energy deviates by −11.9 kcal from the mean.

(23) Integration of electron densities along lines or over volumes and areas has been used previously. Examples include: (a) P. Politzer and R. R. Harris, *J. Am. Chem. Soc.*, **92**, 6451 (1970). (b) R. F. W. Bader and P. M. Beddall, *ibid.*, **95**, 305 (1973). (c) A. Streitwieser, Jr., J. E. Williams, Jr., S. Alexandratos, and J. M. McKelvey, *ibid.*, **98**, 4778 (1976). Streitwieser has used the term electron projection function to describe the line integral of the electron density along a path perpendicular to the molecular plane. (d) K. B. Wiberg, *ibid.*, **102**, 1229 (1980).

Table IV. Total Energies of Proton-Bound Anions (au)

	$X = H_3C^-$	$X = H_2N^-$	$X = HO^-$	$X = F^-$
$XHCH_3^-$	−78.585 491[a]	−94.345 572	−113.866 693	−137.482 368
	−79.530 231[b]	−95.528 372	−115.364 749	−139.378 861
$XHNH_2^-$		−110.103 735	−129.623 211	−153.237 201
		−111.524 683	−131.362 636	−155.374 485
$XHOH^-$			−149.139 171	−172.750 970
			−151.201 189	−175.215 603
XHF^-				−196.359 605
				−199.234 027

[a] Standard 3G basis set, geometries given in Table V. [b] Standard 4-31 basis set.

corresponding to ψ_i. In other words, the orbital energy of each MO and the electron density are partitioned in space in the same proportional manner. Equation 10 is strictly valid only when ψ_i is an exact eigenfunction of the operator H. However, even at the 3G level, gross deviations in electron density distribution and in the relative orbital energies are not expected, and since we are interested in qualitative comparisons, eq 10 has been used as a simple alternative to evaluating the integrand of eq 9 at each point in space.

Plots showing differences in the spatial distribution of orbital energy can be easily constructed by weighting projected electron density plots for each MO with the orbital energy, summing over occupied MOs and forming differences as with Figure 1. An example of such a plot is shown in Figure 2, which can be regarded as a projected orbital energy difference (POED) graph in analogy with the projected electron density difference (PEDD) plot[23] in Figure 1.

Figure 2 is a useful supplement to PEDD plots since the energetic consequences of a charge redistribution can be more easily evaluated. The main point is that the compensation observed in the PEDD plot also comes through in the POED plot. The orbital energy is nonadditive by 1.16 kcal and from Figure 2 it is apparent that this degree of additivity in the total orbital energy is due to cancelation of substantially larger positive and negative deviations in different spatial regions. Each half of the grid in Figure 2 integrates to about |40| kcal.

E. Energy Additivity and the Equivalent Group. Spatial Distribution of Kinetic Energy. Projected kinetic energy difference (PKED) plots can be constructed by integrating

$$dT_i = \psi_i T \psi_i \, d\tau \qquad (11)$$

along the z axis and forming differences between corresponding fragments. Since even the exact ψ_i is not an eigenfunction of the kinetic energy operator, the kinetic energy density is not proportional to the electron density in the same volume element. The properties of the kinetic energy are of interest since it was shown via the virial theorem[12] that total energy additivity occurs to the extent that the kinetic energy is additive. The virial theorem does not apply to the individual regions corresponding to the Ar and Ne fragments,[24] but it is still of interest to examine the contribution of each spatial region to the total kinetic energy. Since compensating shifts in electron density and orbital energy have been previously noted, compensating differences in the PKED plots would also be expected.[25] In Figure 3 this expectation is realized and it can be shown that the additivity in total kinetic energy (−0.10 kcal of the mean) is not due to a nearly constant distribution of kinetic energy over the Ar and Ne regions. Large positive changes (~80 kcal)[26] in the Ar area are canceled by nearly equal negative changes in the Ne area to give excellent overall additivity (0.1 kcal).

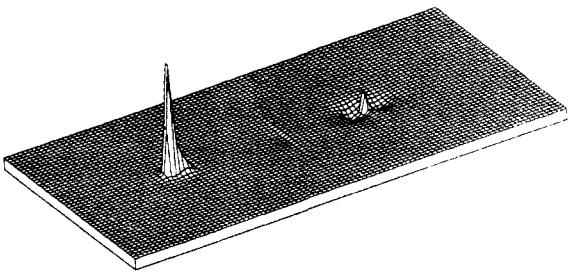

Figure 3. Projected kinetic energy difference plot for $ArHNe^+$. The kinetic energy is evaluated as a function of the spatial coordinates according to eq 11, and projected differences are plotted as in Figure 1. Maximum equals 2.216 au/bohr^2.

F. Additive Total Energy Does Not Require Equivalent Groups. The conclusions are clear. The additivity seen in the calculated total energy for $ArHNe^+$ is not due to transferable groups of nearly constant electronic structure or to additivity of the orbital energy or of the classical electrostatic energy. The electronic environments of the Ar, Ne, and H regions are noticeably different in the hemistructural molecule and in the parents. These changes in electronic structure account for energy differences one to three orders of magnitude larger than the overall deviation from additivity. Additivity is observed because the changes in electronic structure are mutually compensating.

It is important to place the differences in Figures 1–3 in proper perspective. For example, the kinetic energy difference over the Ar fragment in Figure 3 is about 80 kcal. Since the total kinetic energy over the Ar fragment in $ArHNe^+$ is ~327 000 kcal, the perturbation could be regarded as small.[27] From this viewpoint,

(24) Bader has outlined conditions which are sufficient for dividing a molecule into "virial" fragments so that each fragment satisfies the virial theorem (ref 16d).

(25) Bader has also shown that the total kinetic energy within "virial" fragments (ref 24) can be uniquely defined, even though the kinetic energy at a given point is not necessarily unique. Bader has also shown that the kinetic energy of a volume element is a function of the charge density in that element so that the compensating pattern seen in PEDD plots should be repeated in the PKED plots. The significance of the particular distribution represented by eq 11 is that it corresponds to the contribution of each volume element to the kinetic energy expectation value, $\langle \psi_i T \psi_i \rangle$.

(26) The integrations over the area of the grid are performed numerically using Gaussian quadrature or Simpson's rule. The PKED function integrated over the Ar half of the grid gives 0.032169 au. The total kinetic energy difference on the Ar half is 4(0.032169) au, since allowance must be made for the PKED function below the grid (factor of 2) and for two electrons per orbital. The PKED function integrated over the Ne half of the grid gives −0.031988 au, corresponding to a kinetic energy difference of −4(0.031988) au. The total deviation from additivity is given by 4(0.032169 − 0.031988) au = 0.45 kcal which is in reasonable agreement with 0.1 kcal determined by direct calculation.

(27) It was mentioned earlier that the energy difference between $NeHNe^+$ and $ArHAr^+$ amounts to over 495 000 kcal, and one could legitimately wonder about the applicability of perturbation arguments to such a large energy change. However, by employing a "balancing" trick this huge difference can be reduced. It is instructive to compare the energies of the isonuclear and isoelectronic structures [$NeHNe^+$ + Ar + Ar], [$ArHNe^+$ + Ar + Ne], and [$ArHAr^+$ + Ne + Ne]. The total energies of the three structures are[13b] −1295.930139, −1295.895290, and −1295.860773 au, respectively, and the energy range is now about 44 kcal instead of 495 000 kcal. Expressed as a fraction of the total energy, the 44 kcal perturbation is quite small: <0.006%. The changes in Mulliken population (Table III) also indicate a small perturbation: the variations are largest for the valence p_x orbitals of Ar (0.041 e) and Ne(0.031 e) and for the H 1s orbital (0.081 e). Based on two electrons, these changes amount to 4% or less. As one might expect from the small population variations, the changes in density matrix elements are also small. The largest change in diagonal elements is for the H 1s orbital (12%) and the changes for the remaining elements are less than 4%. The pattern is similar for the off-diagonal elements. Overall, these results suggest that treating $NeHNe^+$, $ArHNe^+$, and $ArHAr^+$ in terms of perturbation theory[12] is reasonable. A more complete evaluation of the quantitative applicability of perturbation theory is desirable and is currently in progress.

Table V. Optimized[a] Bond Lengths for Proton-Bound Anions

	r_{XH}, Å			
	$X^c = H_3C^-$	$X^c = H_2N^-$	$X^c = HO^-$	$X^c = F^-$
$XHCH_3^-$	1.3784	1.2018 (+0.0037)[b]	1.0747 (+0.0096)[b]	1.0253 (+0.0642)[b]
$XHNH_2^-$	1.4516	1.2713	1.1208 (+0.0027)[b]	1.0426 (+0.0323)[b]
$XHOH^-$	1.4907	1.3306	1.1774	1.0760 (−0.0001)[b]
XHF^-	1.5313	1.3750	1.2153	1.114

[a] Standard 3G basis set. [b] Deviation of X–Y distance from mean of X–X and Y–Y distances. [c] r_{CH} = 1.1090 Å, ∠HCH = 101.01° (methyl hydrogens, C_3 symmetry). r_{NH} = 1.0310 Å, ∠HNH = 106.7° (all HNH angles). r_{OH} = 0.9660 Å, ∠HOH = 104.5° (bridging HOH angle). Hydrogens on fragments are always in trans, staggered geometries where appropriate.

Ar has a very similar electronic structure in $ArHAr^+$ and in $ArHNe^+$, and the transferable group concept accounts for nearly 99.98% of the total energy. As long as we do not worry about the remaining 0.02%, the transferable group is a reasonable description. However, it is fair to say that the additivity seen for the total kinetic energy of $ArHNe^+$ (0.1 kcal, Table II) has little or nothing to do with the degree of fragment transferability. The 0.1 kcal is due to a near cancelation of large (~80 kcal) positive and negative deviations in separate spatial regions. In this sense, the variations in the spatial distribution of kinetic energy are substantial, and additivity persists in spite of the breakdown in transferability.

G. Variations in Total Energy Follow the Variations in Kinetic Energy. It was shown[12] that the kinetic energy will respond to a perturbation in a simpler fashion than the individual potential energy components (V_{nn}, V_{ne}, and V_{ee}). The fundamental reason for this behavior is that the kinetic energy change can be described solely in terms of the change in wave function since the kinetic energy operator does not change[12] for the type of perturbation represented by the hemistructural relationship. The potential energy variations involve changes in both the operator and wave function. The extra terms associated with the operator ensure a more complicated relationship between V_{ne}, V_{ee}, and V_{nn} than for T.[12] The importance of understanding the behavior of the kinetic energy lies in the fact that if the hemistructural molecule corresponds to an equilibrium geometry or transition state, the total energy ($E = T + V_{ne} + V_{ee} + V_{nn}$) will also equal $-T$. This relationship also requires that $E = V/2$ where $V = V_{ne} + V_{ee} + V_{nn}$. Satisfaction of these constraints requires that the complexities present in the individual terms V_{ne}, V_{ee}, and V_{nn} cancel away in the sum. Since these restrictions do not apply to the orbital energy ($E_0 = T + V_{ne} + 2V_{ee}$) and since V_{nn} and V_{ee} are generally unequal and nonadditive, the orbital energy will be less additive than E, T, or V. These features of the nuclear substitution theory[12] come through in very striking fashion (Table II).

Proton-Bound First Row Anions

In Table IV, energies are reported for XHY^- where X and Y are anions (H_3C^-, H_2N^-, HO^-, F^-). The calculations have been performed using Pople's 3G and 4-31G basis set. It is well known that Hartree–Fock theory gives poor descriptions of anions[28] and that realistic computations must include correlation energy. Nonetheless, certain trends within the calculated properties clearly illustrate some of the features predicted for hemistructural molecules.[12] Consequently, we feel that these results are worth a brief discussion.

The energies reported in Table IV correspond to geometries which have been carefully optimized at the 3-G level with respect to the X–H and H–Y distances. Internal coordinates of the X and Y fragments have not been optimized and correspond to our estimates of reasonable values. The complete fragment geometries are given in Table V. One interesting result is that if the X–H–Y structure contains adjacent atoms in the first row of the periodic table, then the energies show a high degree of additivity. Examples are H_2N–H–CH_3^-, HO–H–NH_2^-, and F–H–OH^- where the deviations from additivity are 0.6, 1.1, 1.0 kcal, respectively. As the X and Y fragments diverge further in structure, additivity begins to break down as seen in the sequence H_2N–H–CH_3^- (0.6 kcal), HO–H–CH_3^- (2.7 kcal), F–H–CH_3^- (6.2 kcal) (Table VI).

Table VI. Energy Additivity (kcal). Proton-Bound Anions

	$X = H_2N^-$	$X = HO^-$	$X = F^-$
$XHCH_3^-$	−0.6[a] −0.6[b]	−2.7[a] +0.6[b]	−6.2[a] +2.1[b]
$XHNH_2^-$		−1.1[a] +0.2[b]	−3.5[a] +3.1[b]
$XHOH^-$			−1.0[a] +1.3[b]

[a] Energy deviation of XHY^- from mean energy of XHX^- and YHX^-; 3G basis set; geometries listed in Table V. [b] Same as a above, except calculations are performed at the 4-31 level.

The 3G basis set predicts the basicity order $F^- > HO^- > H_3C^- > H_2N^-$, which is incorrect[29] and is probably due to the progressively poorer description of the central atom of the anion with increasing nuclear charge. However, it is interesting that the deviations from the hemistructural geometry apparently correlate with the electronegativity of the end atoms. In $X–H–Y^-$ for constant Y, the X–H distance shortens and the H-Y distance lengthens as the difference in electronegativity between X and Y increases. It is especially noteworthy that the H coordinates deviate more from the hemistructural position than the X or Y coordinates. For example, the O–H distance in HO–H–F^- lengthens by 0.0379 Å compared to HO–H–OH^-, while the H–F distance shortens by 0.0380 Å compared to F–H–F^-. As a result, the O–F distance is within 0.0001 Å of the mean O–O and F–F distances. This behavior is somewhat analogous[12] to Johnston's proposal of bond order conservation[30] in transition states of atom-transfer reactions, and has been predicted from an analysis of the nuclear forces at the hemistructural geometry.[12] This pattern holds fairly well for X, Y = O, F; N, O; and C, N and progressively breaks down as X, Y diverge further in structure. It is interesting to note that the deviations are greater for the X–H and Y–H distances than for the X–Y distance, as predicted.[12]

These basic results have also been observed when the calculations are repeated at the 4-31 level. Full geometry optimizations for all systems have not yet been done, but the degree of energy additivity for the hemistructural geometries is fully comparable. Similar results have been noted for other anions (e.g., CH_3O^-, $CH_3CH_2O^-$, HC≡C^-, N≡C^-, HC≡C–CH_2^-, N≡C–CH_2^-) with both 3-G and 4-31 basis sets. Hydride bound cations, including alkyl, cyclopropenyl, and azacyclopropenyl, have also been examined with similar results. The 3-G and 4-31 basis sets have been used in the present study as economic expedients. Energy additivity is not substantially different in the two basis sets, and the 3-G minimal basis set undoubtedly underestimates the changes in electronic structure of the various fragments. As a result, the conclusion that additivity is due to mutual cancelation of positive and negative deviations in different spatial regions is unlikely to require significant revision when these calculations are repeated using more refined theoretical techniques. However, from previous theoretical considerations,[12] there are strong indications that the virial theorem and the Hellmann–Feynman theorem play a key role in this behavior.[12] Consequently, we are interested in obtaining wave functions which satisfy the virial and Hellmann–Feynman theorems and which yield energies close to the Hartree–Fock limit. It will also be important to include correlation effects. The initial stages of this work are now underway with PROMETHEUS X.

(28) W. A. Lathan, L. A. Curtiss, W. J. Hehre, J. B. Lisle, and J. A. Pople, *Prog. Phys. Org. Chem.*, **11**, 175 (1974).

(29) The order calculated in the 4-31 basis set is reversed: $H_3C^- > H_2N^- > HO^- > F^-$.

(30) H. S. Johnston and C. Parr, *J. Am. Chem. Soc.*, **85**, 2544 (1963).

Table VII. Calculated Energy Components for Proton-Bound Anions

	E_o, au	T, au	V_{ne}, au	V_{ex}, au	V_{co}, au	V_{nn}, au	E, au
[b]F H F$^-$	−104.654 026	196.362 699	−539.789 251	−21.583 721	140.969 985	27.677 591	−196.362 699
[c]F H OH$^-$	−93.900 366	172.752 830	−485.994 399	−19.941 768	129.612 370	30.816 317	−172.754 651
[d]HO H OH$^-$	−83.011 915	149.142 551	−432.450 969	−18.306 672	118.454 923	34.017 615	−149.142 551
Δ,[a] kcal	−42.291	0.129	78.884	2.151	−62.803	−19.632	−1.271

[a] Δ represents the deviation of the calculated component of FHOH$^-$ from the mean of the corresponding components for FHF$^-$ and HOHOH$^-$. All values are in kcal. [b] r_{FH} = 2.113 623 24 μ_B; η = 0.996 012 658. [c] r_{FH} = 2.113 623 24 μ_B; r_{HO} = 2.235 868 09 μ_B; r_{OH} = 1.834 418 091 μ_B; ∠HOH = 103.286°, η = 1.000 108 850. [d] r_{HO} = 2.235 868 09 μ_B; r_{OH} = 1.834 418 091 μ_B; ∠HOH = 103.286°; η = 0.995 142 069. The exponents for FHOH$^-$ have been taken from the corresponding orbitals in the symmetrical structures, except for the bridging proton whose exponents are the average of the corresponding exponents for the symmetrical structures. The scaling factor of 1.000 108 850 for FHOH$^-$ indicates that this "hemistructural" basis set was scaled by a factor of (1.000 108 850)^2 to give the energies reported above.

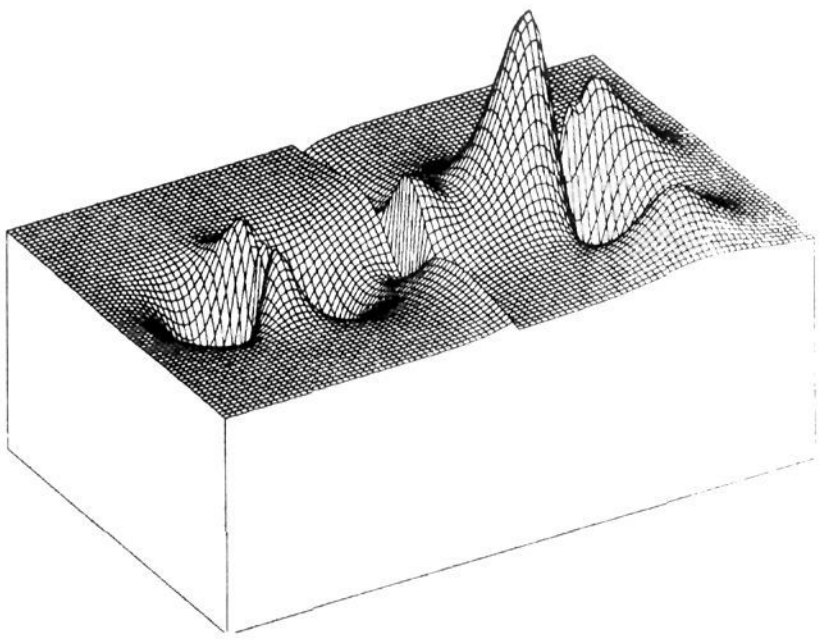

Figure 4. Projected electron density difference plot for F–H–OH$^-$. Maximum equals 0.00517 electron/bohr^2.

As mentioned earlier, F–H–OH$^-$ shows a high degree of energy additivity (∼1 kcal). Before closing, it would be worthwhile to examine this behavior somewhat further. In Table VII, the energies for F-H-F$^-$, F-H-OH$^-$ and HO-H-OH$^-$ are listed. The geometries of the two symmetrical structures were carefully optimized (3G basis) with respect to X–H and H–Y distances. The scaling procedure was then applied to produce the scaling factors and new bond lengths reported in Table VII. The unsymmetrical structure F–H–OH$^-$ was scaled, maintaining the geometry at the hemi-structural positions defined by the final geometries of the scaled F–H–F$^-$ and HO–H–OH$^-$. Since the geometry of F–H–OH$^-$ is not varied during the scaling procedure, the virial theorem is not exactly satisfied, but the error is small (∼1 kcal). The individual potential energies, V_{nn}, V_{ne}, and V_{ee}, are substantially nonadditive (20–80 kcal), while E, T, and V are additive to within 1.4 kcal. The additivity of the orbital energy is relatively poor (∼42 kcal). The exchange energy is additive to within 2.1 kcal, so that the classical electrostatic energy is somewhat less additive than E, T, and V. The overall pattern is similar to that observed for ArHNe$^+$.

The PEDD, POED, and PKED plots for F–H–OH$^-$ are shown in Figures 4–6. As with ArHNe$^+$, the degree of additivity depends on mutual cancelation of large positive and negative deviations in separate spatial regions. For example, the integrated orbital energy difference (Figure 5) over the F fragment yields about −132 kcal, while the corresponding quantity over the OH fragment gives ∼83 kcal. The combined sum is roughly −49 kcal in reasonable agreement with the exact 3G scaled value of −42 kcal. The discrepancy is due to the numerical integration procedure (Simpson's rule) used for integrating the grids. Over the same regions, the integrated kinetic energy difference (Figure 6) is −60 kcal (F) and +62 kcal (OH). The integrated total (2 kcal) is in reasonable agreement with the direct value (0.1 kcal). Once again, it is seen that additivity depends on mutual cancelation of different changes in electronic structure rather than similarity of fragment

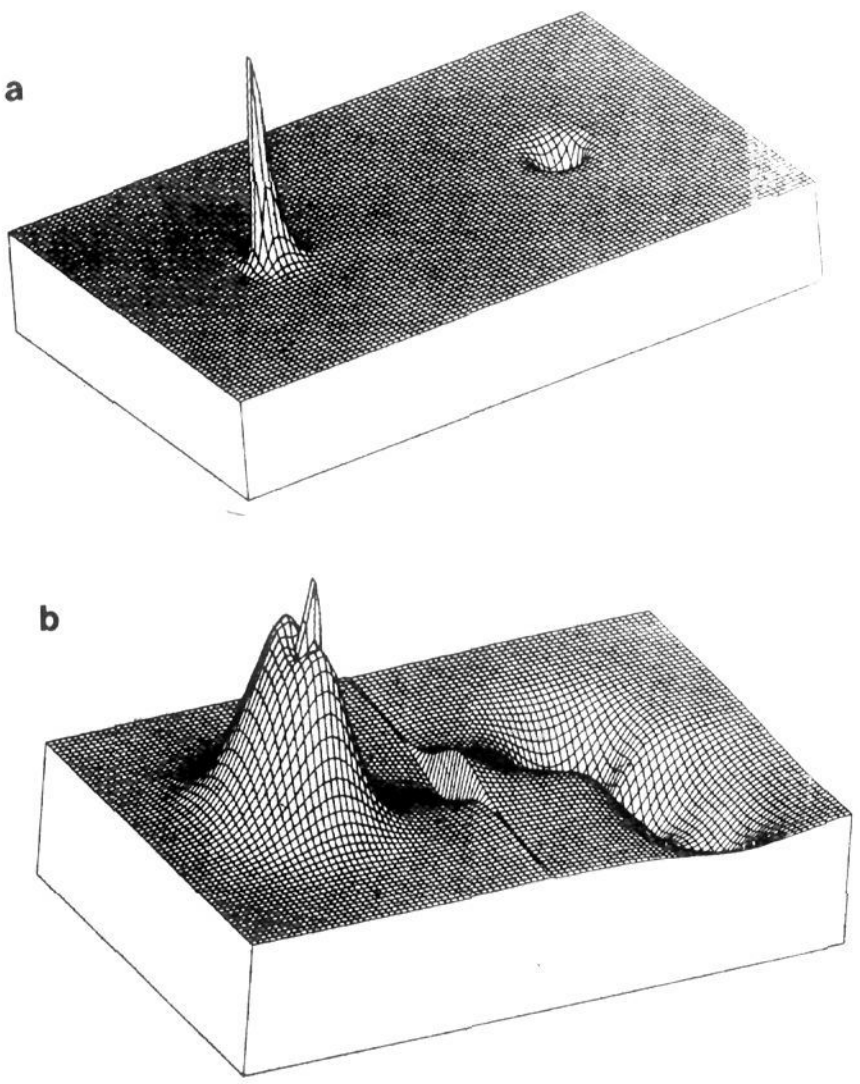

Figure 5. Projected orbital energy difference plot for F–H–OH$^-$. (a) Core orbitals, maximum equals 0.302 au/bohr^2. (b) Valence orbitals, maximum equals 0.027 au/bohr^2. The integration mentioned in the text refers to the combined sum of core and valence orbitals.

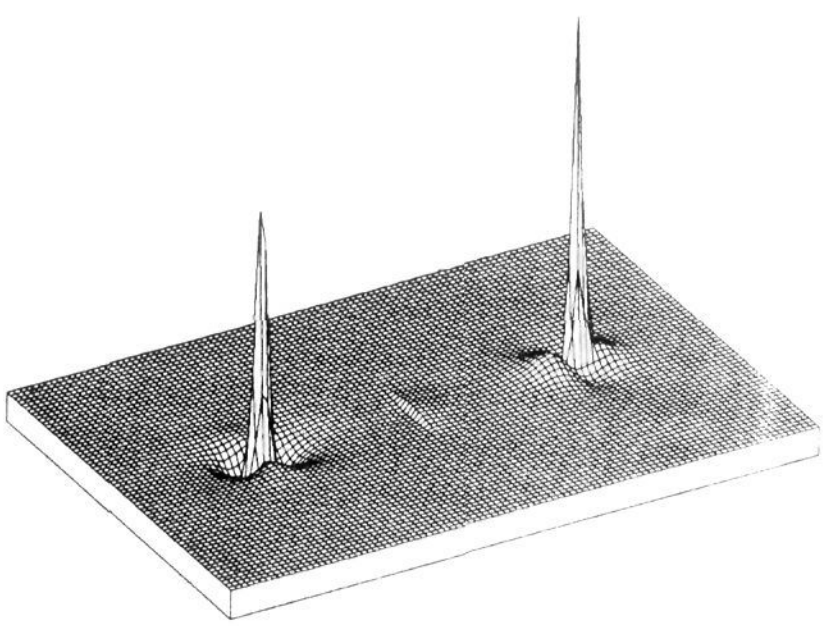

Figure 6. Projected kinetic energy difference plot for F–H–OH$^-$. Maximum equals 0.735 au/bohr^2.

electronic structure in different environments.

The Relationship between Structural Transferability and Energy Additivity

Transferability has often been used to rationalize observations of additivity.[16] For example, Rothenberg[31] has shown that orbitals of methane and ethane can be localized and that one-electron properties of the localized C–H orbitals vary by less than 2–3%. The kinetic energy associated with a C–H orbital in methane is 0.8690 au while the corresponding quantity for ethane in the staggered conformation is 0.886 au.[31] These values are within 2% of each other, but the difference corresponds to about 10 kcal. However, additivity holds to a much higher degree for unbranched saturated hydrocarbons. For example, the total energies[28,32a] of propane (−118.09211 au), ethane (79.11582 au), and methane (−40.13978 au) are additive to within 0.08 kcal (4-31 G basis set). This additivity is not appreciably dependent on basis set and is seen for minimum basis sets as well.[28,32b] This comparison suggests that the degree of transferability seen with localized orbitals is not sufficient to account for the additivity in total energy.

In a similar vein, Degand, Leroy, and Peeters[33] have reproduced orbital energies for methane, ethane, and propane to within 0.1% by transferring Fock matrix elements derived from a basis set of localized orbitals. This comparison emphasizes that transferability is a reasonable description of the total wave functions, but the degree of additivity differs from the corresponding ab initio calculation by over 30 kcal.[33b]

Another method based on transferable Fock matrix elements is the SAMO technique[34a] which has been applied to ethane, propane, and butane. The direct ab initio calculation gives additive total energies to within 0.10 kcal, while the SAMO energies are only additive to 30 kcal.[34b]

Conclusions

In the previous paper,[12] it was demonstrated analytically that energy additivity does not require wave function transferability or constant electronic structure. In the current paper, examples have been presented which show a high degree of additivity in total energy, but not because of constant electronic structure. Large positive kinetic energy deviations (~80 kcal) in one spatial region are offset by comparable negative deviations in other regions to give a total kinetic energy which is additive to 0.1 kcal. The present work has shifted the focus from group transferability to mutual cancelation as the root of energy additivity.

Acknowledgment. This work was supported in part by a grant from the donors of the Petroleum Research Fund, administered by the American Chemical Society, by the Pennwalt Corporation Grant of Research Corporation, by a USPHS Biomedical Research Grant (4-521355-24739), by NSF, and by continued assistance from the University Research Committee (UCLA). J.R.M. also acknowledges a Regents' Junior Faculty Fellowship (1978–1979) and a UCLA Faculty Career Development Award (1979–1980). The authors thank Professors William McMillan, William Gelbart, and Daniel Kivelson and Dr. Peter Ogilby for extensive discussions. The authors would also like to thank Professors Joel Liebman and Paul von Rague Schleyer for preprints and helpful comments.

(31) S. Rothenberg, *J. Am. Chem. Soc.*, **93**, 68 (1971).

(32) (a) L. Radom, W. J. Hehre, and J. A. Pople, *J. Am. Chem. Soc.*, **94**, 2371 (1972). (b) The 3G energies of methane, ethane, and propane are −39.72686, −78.30618, and −116.88580 au (L. Radom and J. A. Pople, *ibid.*, **92**, 4786 (1970)). The additivity is within 0.10 kcal.

(33) (a) Ph. Degand, G. Leroy, and D. Peeters, *Theor. Chim. Acta*, **30**, 243 (1973). (b) The ab initio orbital energies for methane, ethane, and propane are −28.3284, −55.3636, and −82.5678 au. The orbital energy of ethane is 53.02 kcal above the mean orbital energy of methane and propane. In the same basis set (ref 33a), the transferable matrix element procedure gives −28.3000, −55.37980, and −82.5210 au. The absolute values agree reasonably well, but the orbital energy for "transferable" ethane is only 19.26 kcal above the mean.

(34) (a) J. E. Eilers and D. R. Whitman, *J. Am. Chem. Soc.*, **95**, 2067 (1973). (b) The ab initio energies of ethane, propane, and butane are −78.8196, −117.6776, and −156.5353 au. The corresponding SAMO energies are −78.8049, −117.6275, and −156.5479 au.

Catecholate and Phenolate Iron Complexes as Models for the Dioxygenases

Robert H. Heistand II, Randall B. Lauffer, Erol Fikrig, and Lawrence Que, Jr.*

Contribution from the Department of Chemistry, Baker Laboratory, Cornell University, Ithaca, New York 14853. *Received September 28, 1981*

Abstract: The syntheses and physical properties of a series of Fe(salen)X and Fe(saloph)X complexes where X is phenolate or catecholate are reported. Magnetic susceptibility measurements as well as electronic, infrared, and NMR spectra indicate that the catecholate in Fe(salen)catH behaves very much like a phenolate and is concluded to be monodentate in its coordination to the iron. The abstraction of a proton from Fe(salen)catH results in an anionic complex, [Fe(salen)cat]$^-$, with markedly different properties; the catecholate in this complex is chelated. Both monodentate and chelated catecholate complexes are high-spin ferric, demonstrating that catecholate coordination to a bis(phenolato)iron(III) complex does not result in the reduction of the ferric center. This is in agreement with observations made on dioxygenase–substrate complexes. In addition, studies on a series of Fe(salen)X complexes where X is phenolate, thiophenolate, benzoate, and catecholate show that the dominant salen-to-Fe(III) charge-transfer interaction is modulated by the coordination of these ligands. Comparisons with corresponding dioxygenase complexes show that the tyrosinate-to-iron(III) charge-transfer interactions are similarly affected, thus indicating that the salen ligand provides a reasonable approximation of the iron environment in the dioxygenases.

The interaction of molecular oxygen with metalloenzymes is currently an area of considerable activity.[1] One interesting reaction is the dioxygenation of catechols to yield *cis,cis*-muconic acids, catalyzed by the nonheme iron enzymes catechol 1,2-dioxygenase and protocatechuate 3,4-dioxygenase.[2,3] Spectroscopic studies on these enzymes show the active site iron to be a mo-

(1) Hayaishi, O., Ed. "Molecular Mechanisms of Oxygen Activation"; Academic Press: New York, 1974.

(2) Nozaki, M., in ref 1, Chapter 4.

(3) Que, L., Jr. *Struct. Bonding (Berlin)* **1980**, *40*, 39–72.

0002-7863/82/1504-2789$01.25/0